

Enhancing Electric Fields in High-Index Resonators by Flux Conservation of the Displacement Current Density

Bruno Miranda,^{†,‡} Vincenzo D'Ambrosio,[¶] Giovanni Miano,[§] Luca De Stefano,^{||}
and Carlo Forestiere^{*,†}

[†]*Department of Electrical Engineering and Information Technology, Università degli Studi di Napoli Federico II, via Claudio 21, Naples, 80125, Italy.*

[‡]*Institute of Applied Sciences and Intelligent Systems - Unit of Naples, National Research Council, Via P. Castellino 111, Naples, 80131 Italy.*

[¶]*Department of Physics “E. Pancini”, University of Naples Federico II Via Cinthia, I-80126, Naples, Italy.*

[§]*Department of Electrical Engineering and Information Technology, Università degli Studi di Napoli Federico II, via Claudio 21, Napoli, 80125, Italy.*

^{||}*Institute of Applied Sciences and Intelligent Systems - Unit of Naples, National Research Council, Via P. Castellino 111, 80131 Italy.*

E-mail: carlo.forestiere@unina.it

Phone: +39 081 7682007

Abstract

High-index objects constitute nanoscale optical conduits for the displacement current density field as its normal component to the object walls vanishes. In this paper, we demonstrate that by squeezing the section of a high-index ring resonator, the conservation of the flux of displacement current density naturally imposes the enhancement and localization of the electric field in both the interior of the resonators and in the external space. We verify this general principle in high and moderate- index resonators under different excitation conditions.

Keywords

All-dielectric nanoresonators, Silicon nanoresonators, Field enhancement, Field localization

The material composition of an optical resonator may have profound impact on its electromagnetic scattering properties. Metallic nanoresonators, if very small compared to the operation wavelength in vacuum, give rise to plasmonic resonances that can be described within the electroquasistatic approximation of the Maxwell's equations.¹⁻⁵ High local electric fields could be then achieved by means of mechanisms, such as the tip-shape effects in objects with sharp edges or through capacitive coupling in closely spaced metal objects.⁶ Although radiative effects can be also exploited to further enhance the local electric field (e.g.⁷), they usually play a minor role.

Unfortunately the performance of plasmonic devices are hampered by metal dissipation.⁸ The promise of overcoming material losses in plasmonic objects have stimulated the research in high-index dielectric resonators.⁹⁻¹⁴ Silicon-made resonators, in both periodic¹⁵ and non-periodic¹⁶ arrays, have been already proposed as diagnostic platforms for the screening of cancer biomarkers and for the design of chiral sensing platforms.¹⁷⁻²⁰

Contrarily to plasmonic resonators, the resonances in high-index dielectric nanoparticles, much smaller than the wavelength of the incident light, can be successfully modeled by the magnetoquasistatic approximation of the Maxwell's equations, where the normal component of the displacement current density vanishes on the surface of the object.²¹ The existence of such a profound difference between these two types of resonators suggests that strategies inspired by the electroquasistatic model, which are very effective in metal resonators, may not be as good in enhancing local fields in high-index resonators.

Several scientific contributions have already investigated the field enhancement and localization in high/moderate index resonators.^{9,22-24} Some of them have highlighted that electric field *hot spots* are typically localized in the interior of the resonator,²⁵ in sharp contrast with plasmonic resonators. Although, this is certainly an advantage for non-linear applications,²⁶⁻²⁹ it constitutes a limitation when the goal is to enhance the emission from nearby

molecules or quantum emitters. Aware of this limitation, in Ref.³⁰, the authors introduced a clever strategy to generate an *external* hotspot making a slot aperture in a high-index dielectric disk, achieving very significant enhancement of the electric field, based on the action of the so called *toroidal* dipolar mode (or $\text{HEM}_{12\delta}$ in dielectric antenna resonator literature) of a disk. A very effective strategy was proposed also in Ref.³¹ where the authors exploited the jump of the *normal* component of the electric field at the interface between a high-index dielectric material and the air to enhance the electric fields.

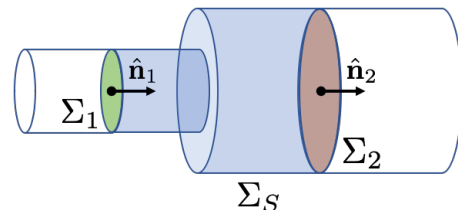


Figure 1: Sketch of a portion of the resonator having varying cross section. Σ_S is a portion of the physical boundary of the resonator, Σ_1 and Σ_2 are purely mathematical surfaces contained in the interior of the resonator.

Given the complementary nature of plasmonic and dielectric resonances, the problem of achieving high field enhancement in high-index objects requires renovated methods, which can be inspired by inherent properties of magnetoquasistatic resonances. *Engheta et al.*³² already envisioned that high-index materials can play the role of nanoscale optical *conduits* for the displacement current density field, analogously to the role that wire conductors play for direct currents in electric circuits. In this paper, we further carry on this analogy, introducing a radically new strategy to achieve high electric field enhancement both in the inside and outside of a high-index resonator. Our strategy is based on the flux conservation of the displacement current density field in dielectric resonators. In fact, as a reduction of the section of a wire conductor entails a local increase of the current density; analogously, a reduction in the section of the high-index material is connected with an increase of the displacement current density and therefore of the electric field.

The platform of choice for the demonstration of this principle is a ring resonator, where the fundamental magnetoquasistatic mode, namely a displacement current density loop associated to a magnetic dipole, is engineered by squeezing the section of the ring, introducing a bottleneck. Because the flux of the displacement current is conserved, the magnitude of the current density has to increase to compensate the decrease of the section. As a result, the electric fields are also enhanced outside of the resonator, thanks to the continuity of the tangential component of the electric field.

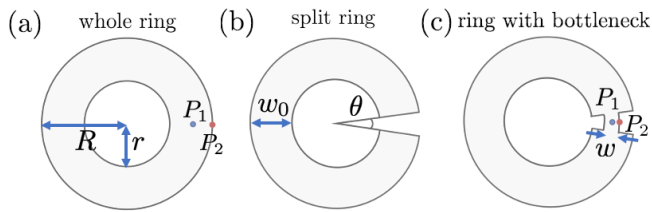


Figure 2: Top view of the three investigated ring resonators: the whole ring (a), the split ring (b) and the ring with a bottleneck (c), with minor radius r , major radius $R = 2r$, and height h . The width of the ring is $w_0 = r$. In the split ring, we removed an angular sector of aperture θ . In (c), the bottleneck has width w .

We apply this principle to high and moderate-index resonators, showing strong localization and enhancement of the electric field, which may be promising for surface-enhanced molecular spectroscopies³³ or single-photon emission enhancement,³⁴ surface-enhanced Raman spectroscopy,³⁵ single-molecular detection and biosensing.^{36,37}

Flux Conservation in High Index Resonators

Let us consider a homogeneous, isotropic, non-magnetic linear material having relative permittivity ε_R . It occupies a bounded domain Ω , with regular boundary $\partial\Omega$. We define its characteristic size l_c as a chosen linear dimension of the object and its size parameter $x = 2\pi l_c/\lambda$, where λ is the vacuum wavelength. Here, we briefly recall some of the properties of magnetoquasistatic resonances of high-index dielectric

objects, introduced in Ref.²¹ These are connected to the eigenvalues of a magnetostatic integral operator \mathcal{L}_m that gives the vector potential as a function of the displacement current density field \mathbf{J}^d :

$$y_n^2 \mathcal{L}_m \{ \mathbf{J}_h^d \} (\tilde{\mathbf{r}}) = \mathbf{J}_h^d (\tilde{\mathbf{r}}) \quad \forall \tilde{\mathbf{r}} \in \tilde{\Omega} \quad (1)$$

with the condition

$$\mathbf{J}_h^d (\tilde{\mathbf{r}}) \cdot \hat{\mathbf{n}} (\tilde{\mathbf{r}}) = 0 \quad \forall \tilde{\mathbf{r}} \in \partial\tilde{\Omega} \quad (2)$$

where

$$\mathcal{L}_m \{ \mathbf{J}^d \} (\tilde{\mathbf{r}}) = \iiint_{\tilde{\Omega}} \frac{\mathbf{J}^d (\tilde{\mathbf{r}}')}{|\tilde{\mathbf{r}} - \tilde{\mathbf{r}}'|} d\tilde{V}' \quad (3)$$

$\tilde{\mathbf{r}} = \mathbf{r}/l_c$, $\tilde{\Omega}$ is the scaled domain, $\partial\tilde{\Omega}$ is the boundary of $\tilde{\Omega}$, $\hat{\mathbf{n}}$ is normal to $\partial\Omega$ pointing in the vacuum region. Equation 1 holds in the weak form in the functional space constituted by the functions which are div-free within Ω and having zero normal component and equipped with the inner product

$$\langle \mathbf{A}, \mathbf{B} \rangle_{\Omega} = \iiint_{\Omega} \mathbf{A} \cdot \mathbf{B} dV \quad (4)$$

The magnetoquasistatic oscillations associated to the current density eigenmodes \mathbf{J}_h^d arise from the interplay between the polarization energy stored in the dielectric and the energy stored in the magnetic field. The spectrum of the magnetoquasistatic operator \mathcal{L}_m is discrete.^{21,38} The current mode \mathbf{J}_h^d resonance is characterized by a real and positive eigenvalue y_n , which is size-independent. The induced current density fields \mathbf{J}_h^d have a non-zero curl within the particle, but are div-free and have a vanishing normal component on the particle surface.

The resonance angular frequency ω_h of the h -th resonance is given by:

$$\omega_h = \frac{c}{l_c \sqrt{\varepsilon_R}} y_n \quad (5)$$

The resonant electric fields \mathbf{E}_h are immediately connected to the eigenvalue y_n and to the displacement current density mode \mathbf{J}_h^d through

the relation:

$$\mathbf{E}_h = \frac{\mu_0 l_c^2}{y_n^2} \mathbf{J}_h^d \quad (6)$$

The normal component of the displacement current density field vanishes on the surface of the object: this immediately implies that the flux of the displacement current density field mode through any portion of the boundary of the high-index resonator vanishes.

In the following, we turn this property into a strategy for enhancing the electric field in high-index resonators. Let us consider a closed surface Σ , which is the union of three sections Σ_1 , Σ_2 , Σ_S such that $\Sigma = \Sigma_1 \cup \Sigma_2 \cup \Sigma_S$, as sketched in Fig.1. Σ_S is a portion of the resonator boundary $\Sigma_S \subset \partial\Omega$, where the normal component of the current density vanishes, while Σ_1 and Σ_2 are purely mathematical surfaces contained in the interior of Ω , with normal unit vector $\hat{\mathbf{n}}_1$ and $\hat{\mathbf{n}}_2$ and surface areas A_1 and A_2 . Therefore, we have:

$$\iint_{\Sigma_1} \mathbf{J}_h^d \cdot \hat{\mathbf{n}}_1 d\tilde{S}' = \iint_{\Sigma_2} \mathbf{J}_h^d \cdot \hat{\mathbf{n}}_2 d\tilde{S}' \quad (7)$$

Eq. 7 holds for any mode h of any high-index resonator. We now make the additional assumption that there exists a density current mode, e.g. $\mathbf{J}_h^d(\mathbf{r})$, which is directed along $\hat{\mathbf{n}}_1$ and $\hat{\mathbf{n}}_2$ on the surfaces Σ_1 and Σ_2 , respectively

$$\mathbf{J}_h^d(\mathbf{r}) = J_{h,i}^d(\mathbf{r}) \hat{\mathbf{n}}_i \quad \mathbf{r} \in \Sigma_i \quad i = 1, 2 \quad (8)$$

and we also assume that the corresponding flux is non-vanishing. In the next section, we show that a high-index ring resonator exhibits topologically protected modes satisfying these hypotheses. By using Eq. 8 in Eq. 7 we obtain:

$$\frac{\langle J_{h,1}^d \rangle_{\Sigma_1}}{\langle J_{h,2}^d \rangle_{\Sigma_2}} = \frac{A_2}{A_1} \quad (9)$$

where $\langle J_{h,i}^d \rangle_{\Sigma_i}$ is the average of $J_{h,i}^d$ on Σ_i . By combining Eqs. 6 with Eq. 9, we directly obtain that

$$\frac{\langle E_{h,1} \rangle_{\Sigma_1}}{\langle E_{h,2} \rangle_{\Sigma_2}} = \frac{A_2}{A_1} \quad (10)$$

where $\langle E_{h,i} \rangle_{\Sigma_i}$ is the average of the electric field on Σ_i . Equation 10 is the central result of

this paper and constitutes a general principle to achieve high field enhancement in high-index resonators. By squeezing the section of the resonator, as schematized in Fig. 2c, the average electric field of the mode increases to keep the flux constant counterbalancing the reduction of the surface area.

Magnetoquasistatic modes

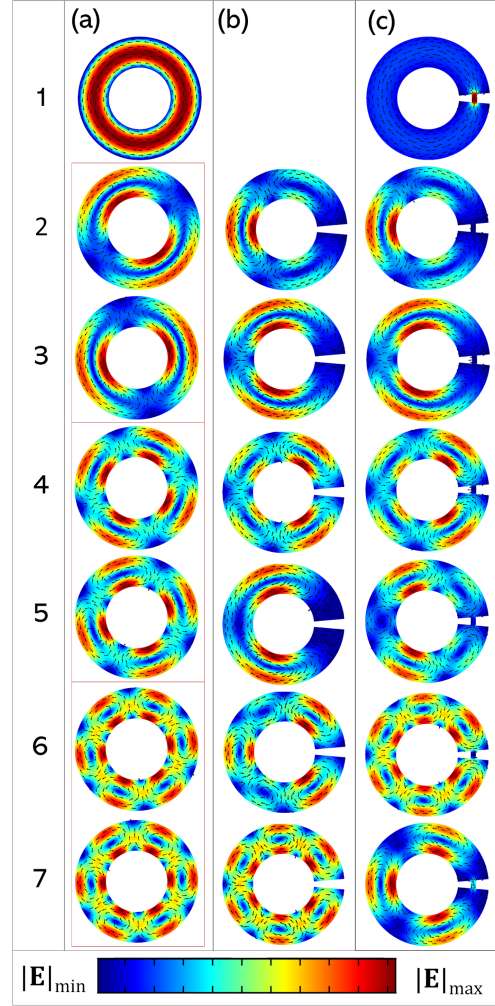


Figure 3: Magnetoquasistatic displacement current density modes of ring resonators with minor radius r , major radius $R = 2r$ and height $h \ll R$. Whole ring (a), split ring (b), and ring with a bottleneck of width $w = w_0/6$ (c). Pairs of degenerate modes are enclosed in red boxes.

Looking for a mode that could be a suitable candidate to apply the flux-conservation design principle, we investigate the magnetoquasistatic modes of a dielectric ring. Dielec-

tric ring resonators have been recently studied experimentally by *Zenin et al.* to control scattering directionality.³⁹ Here, we investigate the ring sketched in Fig. 2a with minor radius r and major radius R , with $R = 2r$, corresponding width $w_0 = R - r = r$, and a thickness h . To simplify our analysis, and only within the current subsection, we make the additional assumption that the ring has thickness h much smaller than R : under this hypothesis we can use the approximated method introduced in Ref.⁴⁰ to calculate the magnetoquasistatic modes of the ring, instead of the three-dimensional but more computationally intensive, method presented in.²¹

The first seven modes exhibited by the ring resonator are shown in Figure 3a. As long as $h \ll l_c$ the current modes are independent of h .

The fundamental mode \mathbf{J}_1^d exhibited by the ring is a displacement current loop circulating along the toroidal direction, shown at the top of Fig. 3a. The next modes are the couple of degenerate modes \mathbf{J}_{2-3}^d associated to two counter-rotating loops of current density field, corresponding to two counter-directed magnetic dipole moments. Higher order modes \mathbf{J}_{4-5}^d \mathbf{J}_{6-7}^d have an increasing number of current loops, where adjacent loops are counter-rotating.

The fundamental mode \mathbf{J}_1^d mode represents the ideal candidate for the proof of concept of the introduced principle because I) the current density is always directed along the toroidal direction and II) the associated flux is non-vanishing. In particular, on the two sections Σ_1 and Σ_2 the displacement current density is directed along the corresponding normal unit vector $\hat{\mathbf{n}}_1$ and $\hat{\mathbf{n}}_2$, respectively. It is worth noticing that the remaining modes \mathbf{J}_{2-8}^d shown in Fig. 3 exhibit a vanishing flux at any section of the ring, and are not useful for our goals.

Thus, we introduce a bottleneck of width w in the ring in correspondence of the angular sector of aperture $\Delta\theta = 10^\circ$ as shown in Fig. 2b. We investigate in Fig. 4 the change of the fundamental magnetoquasistatic mode as the bottleneck reduces w/w_0 in the interval $(1, 0.17)$. As long as the width w of the bottleneck remains finite, the topology of the domain preserves the existence of the loop mode. Moreover, as the

width w is reduced, the amplitude of the displacement current density is enhanced within the bottleneck to keep the flux of \mathbf{J}_1^d constant.

To support this claim, in Fig. 5 we show, with a black line, the relative variation of the flux of the displacement current density of the fundamental magnetoquasistatic \mathbf{J}_1^d between the two sections Σ_1 and Σ_2 , located in the same positions as in Fig. 4 as a function of w/w_0 . In the investigated w/w_0 range, the flux variation, $|\Phi_2 - \Phi_1|/\Phi_1$ is lower than 5%, confirming our design principle.

We also show, in Fig. 3c, the first magnetoquasistatic modes of the ring with the bottleneck of width $w = w_0/6$. The higher-order modes, shown in Figure 3b, are only slightly affected by the introduction of the bottleneck. In particular, the symmetry breaking lifts the degeneracy of the modes in Fig. 3a, but since the net-flux of the corresponding modes through any section of the ring in the column (a) is zero, we do not observe any field localization within the bottleneck.

To further underline the role played in this case by the topology, we also perform a modal analysis on the split ring resonator in Figure 3b. The displacement current density loop embracing the whole structure does not exist in this case, due to the different topology (genus) of the object. The remaining modes are less affected by the change in the topology of the structure.

Full-wave analysis

So far, we have investigated the modes of the ring resonators, which were inherently independent of the excitation conditions. In this section, guided by the previous modal analysis, we turn to the solution of the full-wave 3D scattering problem in the presence of an external excitation using finite-element-method simulations, carried out in COMSOL Multiphysics.

It is important to point out that a plane wave, linearly polarized in the plane of the ring and propagating orthogonally to it, is not able to excite the fundamental loop of the displacement current density, reported in Fig. 4. Nevertheless, thanks to the dephasing, a plane wave propagating within the plane of the ring, or an

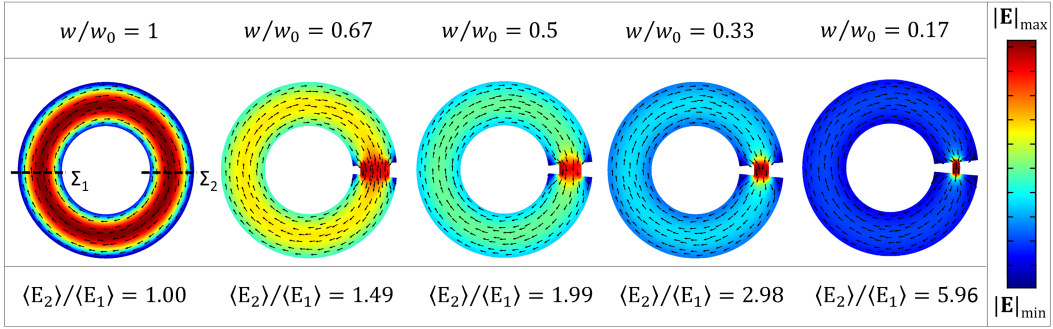


Figure 4: Fundamental magnetoquasistatic mode in ring resonators for rings with bottlenecks of different widths w , in such a way that the ratio w/w_0 is equal to 1 ($w = w_0$ - whole ring), 0.67, 0.5, 0.33, and 0.17. An evident field localization is achieved by decreasing w/w_0 .

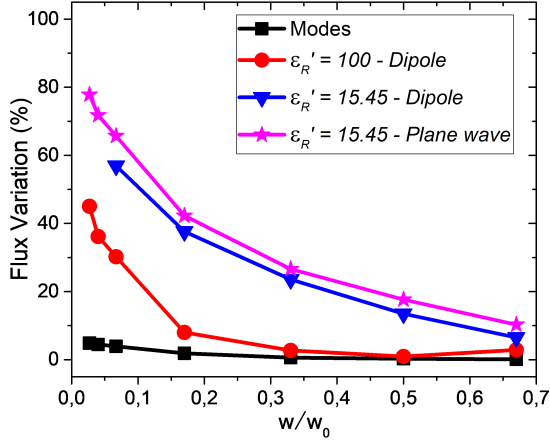


Figure 5: Relative variation of the flux (%) between the cross sections Σ_1 and Σ_2 of the ring resonator as a function of the bottleneck relative width w/w_0 . Σ_1 is located in the unperturbed region, Σ_2 in the middle of the bottleneck. The analysis has been performed for the fundamental magnetoquasistatic modes of a ring ($R = 2r$, $h \ll R$) (black squares) and for the field distribution at the peak obtained by finite element simulation for high-index rings (red circles) ($R = 2r$, $h = R/10$), and silicon rings excited by an electric point dipole (blue triangles) and a plane wave polarized in the plane of the ring (purple stars).

electric dipole located in proximity of the ring may be able to excite it. A dipolar excitation may represent a model of an emitting molecule, a quantum dot, or metal nanoparticle located nearby. In the following, we consider both the aforementioned scenarios.

In Figure 6, we investigate high-index ring resonators with high relative permittivity $\epsilon_R = 100 - 2i$. The ring resonator has rectangular cross section, with minor radius r , major radius $R = 2r$ and thickness $h = R/10$ (see Fig. 2), centered in the origin of a Cartesian coordinate system with its flat faces parallel to the xy plane. In all the investigated cases, to improve numerical convergence, we introduced a smoothing of the bottleneck corners (fillet) with curvature radius of $r/15$. The ring is excited by an electric dipole oriented along \hat{y} and positioned in the point $(-d, 0, 0)$ where $d = 3r$. Besides the *whole* ring, two other geometries are investigated: a *split* ring shown in Fig. 2b where is entirely removed, and a ring where, in correspondence of a sector of angular aperture $\Delta\theta = 10^\circ$, we introduce a bottleneck of width w (Figure 2c). The total electric field $\mathbf{E}_P(\mathbf{r}_P)$, solution of the full-wave electromagnetic problem, is probed in two different points, shown in Fig. 2: the first one is located within the dielectric region in the middle of the bottleneck at the position $\mathbf{r}_{P1} = (r + \frac{w}{2}, 0, 0)$, the second is located in the air at the position $\mathbf{r}_{P2} = (r + \frac{w_0 + w}{2}, 0, 0)$. In these two points, we also calculate the electric field $\mathbf{E}_0(\mathbf{r}_P)$ generated by the exciting dipole, when it is free-standing, namely in the absence of the dielec-

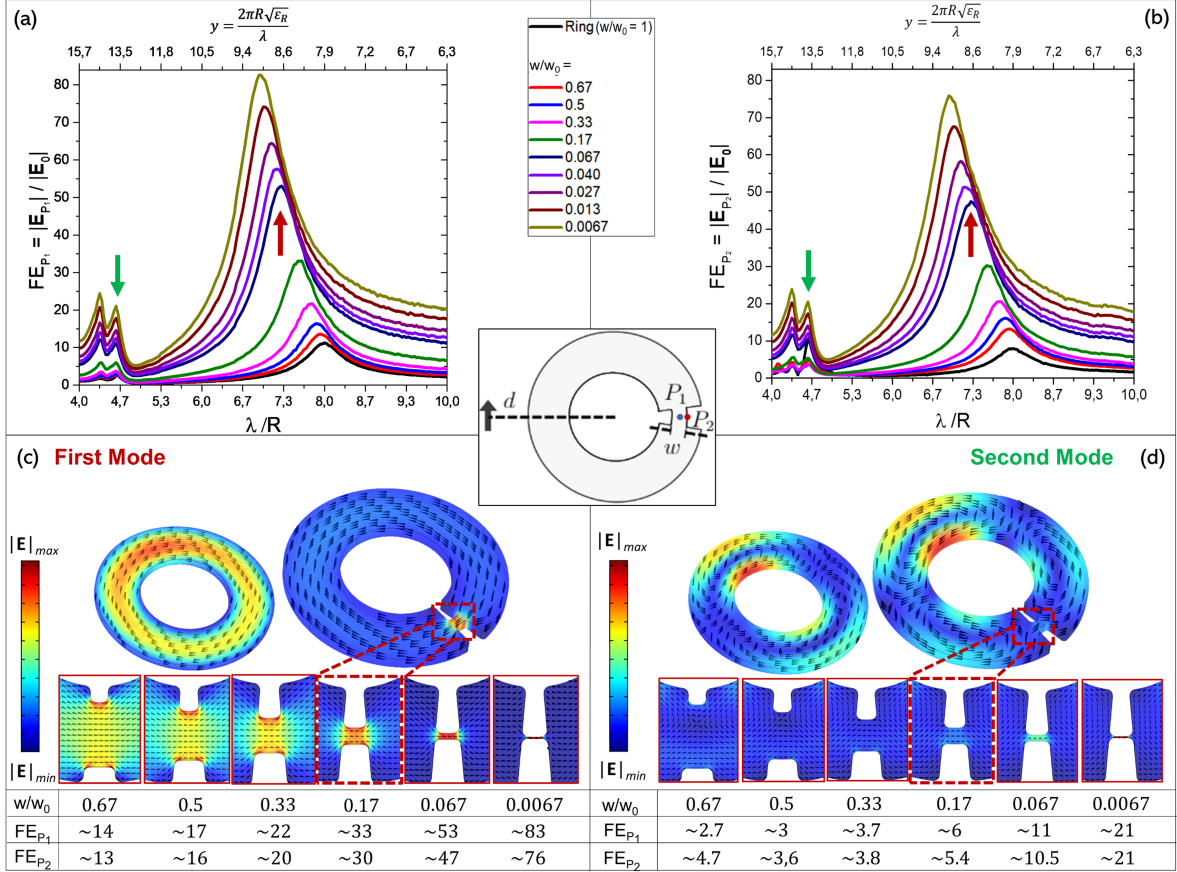


Figure 6: High index ($\epsilon_R = 100 - 2i$) ring resonator with major radius R , minor radius $r = R/2$, thickness $h = R/10$, and bottleneck relative widths w/w_0 , excited by a dipole at a distance d (inset in the Figure). Field enhancements as a function of the free-space wavelength, probed at the points in the dielectric region \mathbf{r}_{P_1} (a), and in vacuum \mathbf{r}_{P_2} (b). The plots also include the field enhancement of the whole ring. Electric field distributions at the fundamental mode resonant peak, indicated by the red arrow, (c) and at the peak of the second resonant mode, indicated by the green arrow, (d) for different w/w_0 values. A zoomed-in view of the bottleneck regions and a table reporting the FE values, corresponding to the different ratios w/w_0 , inside and outside the structures are also included.

tric object. The electric field enhancement FE is defined as the ratio of these two quantities:

$$\text{FE}(\mathbf{r}_P, \lambda) = \frac{\|\mathbf{E}_P(\mathbf{r}_P, \lambda)\|}{\|\mathbf{E}_0(\mathbf{r}_P, \lambda)\|} \quad (11)$$

We show the field enhancement spectrum as a function of the free-space wavelength for the ring with several relative bottleneck widths w/w_0 in correspondence of \mathbf{r}_{P1} (Fig. 6a) and \mathbf{r}_{P2} (Fig. 6b). In both cases, the FE spectrum of the whole ring resonator ($w = w_0$) is also shown for comparison. Since the electric fields of the fundamental mode is tangent to the boundary of the ring, and the tangential component of the electric field are always conserved, the electric field enhancement values in in Fig. 6a are roughly the same of the values in Fig. 6b.

As we reduce the bottleneck width w the peak value of field enhancement increases from $\max_{\lambda} \{\text{FE}(\mathbf{r}_{P1}, \lambda)\} = 11$, for $w = w_0$, to $\max_{\lambda} \{\text{FE}(\mathbf{r}_{P1}, \lambda)\} = 83$, for $w/w_0 = 0.0067$. The peak position undergoes a blue shift, as also expected by the modal analysis.

Figure 6c shows the electric field distribution within the bottleneck of the investigated high-index resonator, which increases by reducing the ratio w/w_0 .

In Fig. 5, we calculate the variation of the flux of the electric field between two cross sections of the ring. It is worth to note that, differently from what we did in the previous section, here the analysis is performed on the state of the electric field, and not on the modes. We choose two sections Σ_1 and Σ_2 , as shown in Fig. 4: Σ_1 in the proximity of the bottleneck, while Σ_2 crossing the bottleneck at its midpoint. We conclude that for $w \geq 0.15w_0$ the flux undergoes a variation of less than 10%. Consistent violations of the flux conservation happen only for values of w less than $0.1w_0$.

We now also analyze the second mode (see Fig. 3), which is associated to the second peak appearing at higher frequencies, in Figure 6a-b. This mode exhibits vanishing flux at any section of the ring, therefore, in this case, the flux conservation does not imply field enhancement. As expected, the field enhancement is significantly lower. An appreciable increase of the

field enhancement is obtained only when the ratio w/w_0 reaches very low values (less than 0.067), but this is mainly due to the partial overlap with the first mode. The field distributions in correspondence of the second peak (from the right to the left), in Figure 6d supports our thesis.

Although permittivities of values 100 and higher are routinely available at microwaves frequencies for several applications including filters, resonators and antennas,⁴¹⁻⁴⁴ in the visible or near infrared only materials with moderate permittivities, such as Silicon or GaAs are currently available. In the following, we consider silicon rings, with $\epsilon_R = 15.45 - 0.1456i$. The ring resonator has major radius $R = 100$ nm, minor radius $r = R/2$, thickness $h = 100$ nm, and different bottleneck widths w/w_0 . In this case, the hypotheses behind the magnetoquasistatic approximation are not fully verified, and a non-vanishing normal component of the displacement current density \mathbf{J}_1^d to the boundary of the particle arises, causing a dispersion of the flux of \mathbf{J}_1^d and a consequent reduction of the maximum achievable field enhancement.

In Fig. 7, we plot the field enhancement as a function of the incident wavelength in free-space spanning between 400 and 1200 nm, corresponding to $y \in [2.09, 6.28]$. In figure 7a, the field enhancement FE is reported.

It is immediately apparent that the values of field enhancement reached by introducing a bottleneck in the silicon ring are lower. For instance, the field enhancement FE obtained for $w/w_0 = 0.067$ is about $25\times$, compared to about $50\times$ achieved in the previous case. This is because, for objects of moderate permittivities, the hypotheses behind the magnetoquasistatic approximation are not fully verified, and a non-vanishing normal component of the displacement current density \mathbf{J}_1^d to the boundary of the particle arises, causing a dispersion of the flux of \mathbf{J}_1^d and a consequent reduction of the maximum achievable field enhancement. To substantiate this claim we show in Fig. 5 the variation of the flux between two sections of the ring. For a bottleneck of section $w = 0.2w_0 = 10nm$, about 40% of the flux is dispersed.

Although the electric dipole, considered so

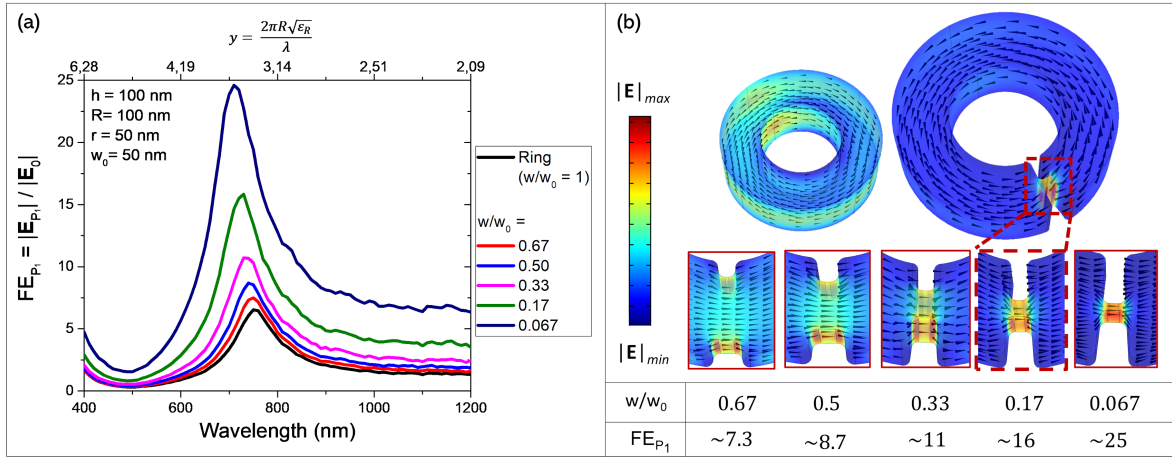


Figure 7: Moderate index ($\epsilon_R = 15.45 - 0.1456i$) ring resonator with major radius $R = 100$ nm, minor radius $r = R/2$, thickness $h = 100$ nm, and different bottleneck widths w/w_0 , excited by a dipole as exemplified in Fig. 1. (a) Field enhancement as a function of the free-space wavelength, probed in the dielectric region at the point \mathbf{r}_{P_1} . The plot also includes the field enhancement of the whole ring. (b) Electric field distribution at the resonant peak of the fundamental mode for different bottleneck width ratios w/w_0 . A zoomed-in view of the bottleneck regions and a table reporting the FE values, corresponding to the different ratios w/w_0 , inside the structures are also included.

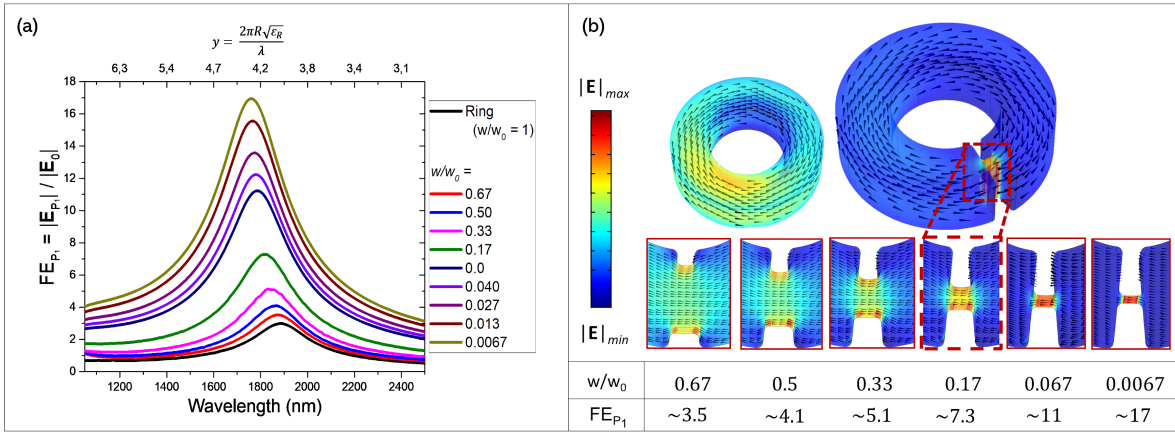


Figure 8: Moderate-index ($\epsilon_R = 15.45 - 0.1456i$) silicon ring resonator with major radius $R = 300$ nm, minor radius $r = R/2$, thickness $h = 160$ nm, and different bottleneck widths w/w_0 in the range $[0.0067, 1]$, excited by a plane wave polarized along x and propagating in the plane of the ring in the y direction. (a) Field enhancement as a function of the free-space wavelength, probed in the dielectric region, in correspondence of \mathbf{r}_{P_1} . The plot also includes the field enhancement of the whole ring. (b) Electric field distribution at the resonant peak of the fundamental mode for different bottleneck width ratios w/w_0 . A zoomed-in view of the bottleneck regions and a table reporting the FE values, corresponding to the different ratios w/w_0 , inside the structures are also included.

far as excitation, may be in principle practically implemented by an emitting molecule, a

quantum dot, or metal nanoparticle small compared to the wavelength, this may be challeng-

ing to implement experimentally, therefore here we also provide the analysis of the implemented resonator when it is illuminated a plane wave linearly polarized along x and propagating in the plane of the ring in the y direction. During its in-plane propagation the electric field undergoes a dephasing, which enables the excitation of the fundamental current density mode. We consider a silicon ring with $R = 300$ nm $r = 150$ nm, $h = 160$ nm and $w_0 = r$. The fundamental mode of the whole ring ($w/w_0 = 1$) is excited at $\lambda_{max} = 1940$ nm. In Fig. 8 we plot the field enhancement in the point \mathbf{r}_{P1} , within the bottleneck, as a function of the incident wavelength in free-space spanning between 1050 and 2500 nm. Also in this case we note that, by reducing the relative bottleneck width, a stronger localization and enhancement of the electric field is obtained, as apparent from Fig. 8b.

Conclusions

The operation of metal and high-index resonators is governed by two complementary long-wavelength limits of the Maxwell's equations, therefore the mechanisms behind the electric field localization and enhancement are expected to be inherently different. Specifically, resonances in high-index small dielectric objects can be modeled by the magnetoquasistatic approximation of the Maxwell's equations, where the normal component of the displacement current vanishes on the surface of the object. As a consequence, the flux through any portion of the resonator boundary vanishes.

In this letter, we demonstrated that by squeezing the section of a high-index resonator, the conservation of the flux of the displacement current density dictates enhancement and localization of the electric field. We apply this design principle to a high-index ring resonator, showing that by squeezing its section through the introduction of a bottleneck, the displacement current density in correspondence of the bottleneck is increasingly enhanced as the width is reduced to keep the flux constant. Furthermore, due to the boundary conditions, the enhancement of the field is achieved in both the

internal and external regions. Then, we consider a ring made of a moderate-index dielectric, where the hypotheses behind the magnetoquasistatic approximation are only partially verified. Even though the achieved enhancement is reduced with respect to the previous ideal case, it is still very significant and comparable in magnitude to alternative status-of-the-art approaches based on electric toroidal dipole resonances.

References

- (1) Fredkin, D. R.; Mayergoyz, I. D. Resonant Behavior of Dielectric Objects (Electrostatic Resonances). *Phys. Rev. Lett.* **2003**, *91*, 253902.
- (2) Bergman, D. J.; Stockman, M. I. Surface Plasmon Amplification by Stimulated Emission of Radiation: Quantum Generation of Coherent Surface Plasmons in Nanosystems. *Phys. Rev. Lett.* **2003**, *90*, 027402.
- (3) Li, K.; Stockman, M. I.; Bergman, D. J. Self-Similar Chain of Metal Nanospheres as an Efficient Nanolens. *Phys. Rev. Lett.* **2003**, *91*, 227402.
- (4) Wang, F.; Shen, Y. R. General Properties of Local Plasmons in Metal Nanostructures. *Phys. Rev. Lett.* **2006**, *97*, 206806.
- (5) Klimov, V. *Nanoplasmonics*; CRC press, 2014.
- (6) Schuller, J. A.; Barnard, E. S.; Cai, W.; Jun, Y. C.; White, J. S.; Brongersma, M. L. Plasmonics for extreme light concentration and manipulation. *Nature materials* **2010**, *9*, 193–204.
- (7) Forestiere, C.; Pasquale, A. J.; Capretti, A.; Miano, G.; Tamburino, A.; Lee, S. Y.; Reinhard, B. M.; Dal Negro, L. Genetically Engineered Plasmonic Nanoarrays. *Nano Letters* **2012**, *12*, 2037–2044, PMID: 22381056.

- (8) Khurgin, J. B. How to deal with the loss in plasmonics and metamaterials. *Nature Nanotechnology* **2015**, *10*, 2–6.
- (9) García-Etxarri, A.; Gómez-Medina, R.; Froufe-Pérez, L. S.; López, C.; Chantada, L.; Scheffold, F.; Aizpurua, J.; Nieto-Vesperinas, M.; Sáenz, J. J. Strong magnetic response of submicron silicon particles in the infrared. *Optics express* **2011**, *19*, 4815–4826.
- (10) Evlyukhin, A. B.; Novikov, S. M.; Zywiets, U.; Eriksen, R. L.; Reinhardt, C.; Bozhevolnyi, S. I.; Chichkov, B. N. Demonstration of Magnetic Dipole Resonances of Dielectric Nanospheres in the Visible Region. *Nano Letters* **2012**, *12*, 3749–3755, PMID: 22703443.
- (11) Kuznetsov, A. I.; Miroshnichenko, A. E.; Fu, Y. H.; Zhang, J.; Luk'yanchuk, B. Magnetic light. *Scientific reports* **2012**, *2*, 492.
- (12) Kuznetsov, A. I.; Miroshnichenko, A. E.; Brongersma, M. L.; Kivshar, Y. S.; Luk'yanchuk, B. Optically resonant dielectric nanostructures. *Science* **2016**, *354*.
- (13) Rybin, M. V.; Koshelev, K. L.; Sadrieva, Z. F.; Samusev, K. B.; Bogdanov, A. A.; Limonov, M. F.; Kivshar, Y. S. High- Q Supercavity Modes in Subwavelength Dielectric Resonators. *Phys. Rev. Lett.* **2017**, *119*, 243901.
- (14) Jahani, S.; Jacob, Z. All-dielectric metamaterials. *Nature nanotechnology* **2016**, *11*, 23.
- (15) Yavas, O.; Svedendahl, M.; Dobosz, P.; Sanz, V.; Quidant, R. On-a-chip biosensing based on all-dielectric nanoresonators. *Nano letters* **2017**, *17*, 4421–4426.
- (16) Yavas, O.; Svedendahl, M.; Quidant, R. Unravelling the Role of Electric and Magnetic Dipoles in Biosensing with Si Nanoresonators. *ACS nano* **2019**, *13*, 4582–4588.
- (17) Hanifeh, M.; Albooyeh, M.; Capolino, F. Helicity Maximization Below the Diffraction Limit. 2019.
- (18) Graf, F.; Feis, J.; Garcia-Santiago, X.; Wegener, M.; Rockstuhl, C.; Fernandez-Corbaton, I. Achiral, Helicity Preserving, and Resonant Structures for Enhanced Sensing of Chiral Molecules. *ACS Photonics* **2019**, *6*, 482–491.
- (19) Mohammadi, E.; Tavakoli, A.; Dekhoda, P.; Jahani, Y.; Tsakmakidis, K. L.; Tittl, A.; Altug, H. Accessible superchiral near-fields driven by tailored electric and magnetic resonances in all-dielectric nanostructures. *ACS Photonics* **2019**, *6*, 1939–1946.
- (20) Garcia-Guirado, J.; Svedendahl, M.; Puigdollers, J.; Quidant, R. Enhanced chiral sensing with dielectric nano-resonators. *Nano Letters* **2019**,
- (21) Forestiere, C.; Miano, G.; Rubinacci, G.; Pascale, M.; Tamburrino, A.; Tricarico, R.; Ventre, S. Magnetoquasistatic resonances of small dielectric objects. *Phys. Rev. Research* **2020**, *2*, 013158.
- (22) Luk'yanchuk, B.; Paniagua-Domínguez, R.; Kuznetsov, A. I.; Miroshnichenko, A. E.; Kivshar, Y. S. Hybrid anapole modes of high-index dielectric nanoparticles. *Physical Review A* **2017**, *95*, 063820.
- (23) Wang, W.; Zhao, X.; Xiong, L.; Zheng, L.; Shi, Y.; Liu, Y.; Qi, J. Broken symmetry theta-shaped dielectric arrays for a high Q -factor Fano resonance with anapole excitation and magnetic field tunability. *OSA Continuum* **2019**, *2*, 507–517.
- (24) Mignuzzi, S.; Vezzoli, S.; Horsley, S. A. R.; Barnes, W. L.; Maier, S. A.; Sapienza, R. Nanoscale Design of the Local Density of Optical States. *Nano Letters* **2019**, *19*, 1613–1617, PMID: 30786717.
- (25) Kapitanova, P.; Ternovski, V.; Miroshnichenko, A.; Pavlov, N.; Belov, P.;

- Kivshar, Y.; Tribelsky, M. Giant field enhancement in high-index dielectric sub-wavelength particles. *Scientific reports* **2017**, *7*, 1–8.
- (26) Grinblat, G.; Li, Y.; Nielsen, M. P.; Oulton, R. F.; Maier, S. A. Enhanced third harmonic generation in single germanium nanodisks excited at the anapole mode. *Nano letters* **2016**, *16*, 4635–4640.
- (27) Ghirardini, L.; Marino, G.; Gili, V. F.; Favero, I.; Rocco, D.; Carletti, L.; Locatelli, A.; De Angelis, C.; Finazzi, M.; Celebrano, M.; Neshev, D. N.; Leo, G. Shaping the Nonlinear Emission Pattern of a Dielectric Nanoantenna by Integrated Holographic Gratings. *Nano Letters* **2018**, *18*, 6750–6755, PMID: 30277790.
- (28) Carletti, L.; Marino, G.; Ghirardini, L.; Gili, V. F.; Rocco, D.; Favero, I.; Locatelli, A.; Zayats, A. V.; Celebrano, M.; Finazzi, M.; Leo, G.; De Angelis, C.; Neshev, D. N. Nonlinear Goniometry by Second-Harmonic Generation in AlGaAs Nanoantennas. *ACS Photonics* **2018**, *5*, 4386–4392.
- (29) Koshelev, K.; Kruk, S.; Melik-Gaykazyan, E.; Choi, J.-H.; Bogdanov, A.; Park, H.-G.; Kivshar, Y. Subwavelength dielectric resonators for nonlinear nanophotonics. *Science* **2020**, *367*, 288–292.
- (30) Yang, Y.; Zenin, V. A.; Bozhevolnyi, S. I. Anapole-Assisted Strong Field Enhancement in Individual All-Dielectric Nanostructures. *ACS Photonics* **2018**, *5*, 1960–1966.
- (31) Robinson, J. T.; Manolatou, C.; Chen, L.; Lipson, M. Ultrasmall mode volumes in dielectric optical microcavities. *Physical review letters* **2005**, *95*, 143901.
- (32) Engheta, N. Circuits with light at nanoscales: optical nanocircuits inspired by metamaterials. *Science* **2007**, *317*, 1698–1702.
- (33) Li, Y.; Su, L.; Shou, C.; Yu, C.; Deng, J.; Fang, Y. Surface-enhanced molecular spectroscopy (SEMS) based on perfect-absorber metamaterials in the mid-infrared. *Scientific reports* **2013**, *3*, 1–8.
- (34) Tapar, J.; Kishen, S.; Prashant, K.; Nayak, K.; Emani, N. K. Enhancement of the optical gain in GaAs nanocylinders for nanophotonic applications. *Journal of Applied Physics* **2020**, *127*, 153102.
- (35) Caldarola, M.; Albella, P.; Cortés, E.; Rahmani, M.; Roschuk, T.; Grinblat, G.; Oulton, R. F.; Bragas, A. V.; Maier, S. A. Non-plasmonic nanoantennas for surface enhanced spectroscopies with ultra-low heat conversion. *Nature communications* **2015**, *6*, 1–8.
- (36) Pryce, I. M.; Kelaita, Y. A.; Aydin, K.; Atwater, H. A. Compliant metamaterials for resonantly enhanced infrared absorption spectroscopy and refractive index sensing. *ACS nano* **2011**, *5*, 8167–8174.
- (37) Bontempi, N.; Chong, K. E.; Oulton, H. W.; Staude, I.; Choi, D.-Y.; Alessandri, I.; Kivshar, Y. S.; Neshev, D. N. Highly sensitive biosensors based on all-dielectric nanoresonators. *Nanoscale* **2017**, *9*, 4972–4980.
- (38) Forestiere, C.; Miano, G.; Rubinacci, G. Resonance frequency and radiative Q-factor of plasmonic and dielectric modes of small objects. 2020.
- (39) Zenin, V.; Garcia-Ortiz, C.; Evlyukhin, A.; Yang, Y.; Malureanu, R.; Novikov, S.; Coello, V.; Chichkov, B.; Bozhevolnyi, S.; Lavrinenko, A.; Mortensen, N. Engineering nanoparticles with pure high-order multipole scattering. *ACS Photonics* **2020**, *7*, 1067–1075.
- (40) Forestiere, C.; Gravina, G.; Miano, G.; Pascale, M.; Tricarico, R. Electromagnetic modes and resonances of two-dimensional

bodies. *Physical Review B* **2019**, *99*, 155423.

- (41) Richtmyer, R. Dielectric resonators. *Journal of Applied Physics* **1939**, *10*, 391–398.
- (42) Kajfez, D.; Guillon, P., et al. *Dielectric resonators*; Noble Publishing Corporation Atlanta, 1998.
- (43) Long, S.; McAllister, M.; Liang Shen, The resonant cylindrical dielectric cavity antenna. *IEEE Transactions on Antennas and Propagation* **1983**, *31*, 406–412.
- (44) Mongia, R. K.; Bhartia, P. Dielectric resonator antennas: a review and general design relations for resonant frequency and bandwidth. *International Journal of Microwave and Millimeter-Wave Computer-Aided Engineering* **1994**, *4*, 230–247.

Graphical TOC Entry

